



# A quantum energy transport model for semiconductor device simulation

Shohiro Sho<sup>a,\*</sup>, Shinji Odanaka<sup>b</sup>

<sup>a</sup> Graduate School of Information Science and Technology, Osaka University, Osaka, Japan

<sup>b</sup> Computer Assisted Science Division, Cybermedia Center, Osaka University, Osaka, Japan

## ARTICLE INFO

### Article history:

Received 1 February 2012

Received in revised form 7 September 2012

Accepted 30 October 2012

Available online 19 November 2012

### Keywords:

Simulation

Numerical method

Quantum energy transport model

Semiconductor

## ABSTRACT

This paper describes numerical methods for a quantum energy transport (QET) model in semiconductors, which is derived by using a diffusion scaling in the quantum hydrodynamic (QHD) model. We newly derive a four-moments QET model similar with a classical ET model. Space discretization is performed by a new set of unknown variables. Numerical stability and convergence are obtained by developing numerical schemes and an iterative solution method with a relaxation method. Numerical simulations of electron transport in a scaled MOSFET device are discussed. The QET model allows simulations of quantum confinement transport, and nonlocal and hot-carrier effects in scaled MOSFETs.

© 2012 Elsevier Inc. All rights reserved.

## 1. Introduction

The semiconductor devices are scaled down into the nanoscale regime to achieve high circuit performance in the future integrated system. The performance of nanoscale semiconductor devices primarily relies on carrier transport properties in the short channels. Quantum energy transport (QET) models have been developed to understand such physical phenomena in scaled semiconductor devices. A full QET model has been derived from the collisional Wigner–Boltzmann equations using the entropy minimization principle [1]. Numerical simulations using this model, however, have not been performed [2]. Simplified QET models have been proposed as the energy transport extension of the quantum drift diffusion (QDD) model with Fourier law closure and numerically investigated [3,4]. In Ref. [4], the carrier temperature in the current density is further approximated by the lattice temperature to bring the model into a self-adjoint form.

In this paper, we develop numerical methods for a QET model derived from a quantum hydrodynamic (QHD) model. To overcome the difficulties associated with the Fourier law closure, we newly derive a four-moments QET model similar with a classical energy transport (ET) model [5]. The numerical stability is achieved by developing numerical schemes and an iterative solution method in terms of a new set of variables. Numerical results in a scaled MOSFET are demonstrated.

The paper is organized as follows: In Section 2, a four-moments QET model is derived from the QHD model. In Section 3, we present nonlinear discretization schemes and an iterative solution method to solve the QET system. In Section 4, numerical simulations of electron transport in a scaled MOSFET are discussed. Some conclusions are addressed in Section 5.

## 2. 4 Moments quantum energy transport model

The QET models are obtained by using a diffusion scaling in the quantum hydrodynamic equations, similar as in the classical hydrodynamic model [5]. The QHD model has been derived from the collisional Wigner–Boltzmann equations, assuming

\* Corresponding author.

E-mail address: [shoshohiro@gmail.com](mailto:shoshohiro@gmail.com) (S. Sho).

Fourier law closure [6]. For classical hydrodynamic simulations, the closure relation based on the four-moments of the Boltzmann equation has been discussed [7–9], and the four-moments ET models are developed for simulations of thin body MOS-FETs [5,10]. In this work, we derive a four-moments QET model from four moments equations derived from the collisional Wigner–Boltzmann equation.

For simplicity, we consider only the case of electrons. The four moment equations have the same form as the classical hydrodynamic equations [7],

$$\partial_t n + \nabla \cdot (n\mathbf{v}) = nC_n, \quad (1)$$

$$\partial_t (n\mathbf{p}) + \nabla \cdot (nU) - n\mathbf{F}_E = nC_p, \quad (2)$$

$$\partial_t (nw) + \nabla \cdot (n\mathbf{S}) - n\mathbf{v} \cdot \mathbf{F}_E = nC_\epsilon, \quad (3)$$

$$\nabla \cdot (nR) - n(wI + U) \cdot \mathbf{F}_E = nC_{p\epsilon}, \quad (4)$$

where  $n$ ,  $\mathbf{p}$ , and  $w$  are the electron density, momentum, and kinetic energy, respectively.  $\mathbf{v}$ ,  $U$ ,  $\mathbf{S}$  and  $R$  are the velocity, second moment tensor, energy flow, and fourth moment tensor, respectively.  $I$  is the identity tensor.  $F_E = -qE$ , where  $E$  is the electric field.  $C_n$ ,  $C_p$ ,  $C_\epsilon$ , and  $C_{p\epsilon}$  are the electron generation rate, the production of crystal momentum, the energy production, and the production of the energy flux, respectively. (1), (2), (3), and (4) represent conservation of particles, momentum, energy, and energy flux, respectively. By assuming parabolic bands, we give the following closure relations for  $\mathbf{p}$  and  $U$  as

$$\mathbf{p} = m\mathbf{v}, \quad (5)$$

$$U_{ij} = mv_i v_j - \frac{P_{ij}}{n}, \quad (6)$$

where  $m$  is an effective mass. The quantum correction to the stress tensor  $P_{ij}$  was proposed by Ancona and Iafrate [11], and the quantum correction to the energy density  $W = nw$  was first derived by Wigner [12], which are given by

$$P_{ij} = -nkT_n \delta_{ij} + \frac{\hbar^2}{12m} n \frac{\partial^2}{\partial x_i \partial x_j} \log n + O(\hbar^4), \quad (7)$$

$$W = \frac{1}{2} mn v^2 + \frac{3}{2} nkT_n - \frac{\hbar^2}{24m} n \frac{\partial^2}{\partial x_k^2} \log n + O(\hbar^4), \quad (8)$$

where  $T_n$  and  $\hbar$  are the electron temperature and Plank's constant, respectively.

For the collision terms, we employ a macroscopic relaxation time approximation to drive a QET model as follows:

$$C_n = 0, \quad (9)$$

$$C_p = -\frac{\mathbf{p}}{\tau_p}, \quad (10)$$

$$C_\epsilon = -\frac{w - w_0}{\tau_\epsilon}, \quad (11)$$

where  $\tau_p$  and  $\tau_\epsilon$  are the momentum and energy relaxation times, respectively. Substituting (5)–(7) into (1) and (2), we obtain moment equations for conservation of electron number and momentum

$$\frac{\partial n}{\partial t} + \frac{\partial}{\partial x_i} (nv_i) = 0, \quad (12)$$

$$\frac{\partial}{\partial t} (mnv_i) + \frac{\partial}{\partial x_j} \left( mnv_i v_j + knT_n - \frac{\hbar^2}{12m} n \frac{\partial^2}{\partial x_i \partial x_j} \log n \right) = -n \frac{\partial V}{\partial x_i} - \frac{mnv_i}{\tau_p}. \quad (13)$$

We further get the following relation:

$$\frac{\partial}{\partial x_i} n \frac{\partial^2}{\partial x_i \partial x_j} \log n = 2n \frac{\partial}{\partial x_j} \frac{1}{\sqrt{n}} \frac{\partial^2}{\partial x_i^2} \sqrt{n}. \quad (14)$$

With the relation (14), the quantum correction term in (13) is written as

$$-\frac{\hbar^2}{12m} \frac{\partial}{\partial x_i} n \frac{\partial^2}{\partial x_i \partial x_j} \log n = -\frac{\hbar^2 n}{6m} \frac{\partial}{\partial x_i} \left( \frac{1}{\sqrt{n}} \frac{\partial^2}{\partial x_j^2} \sqrt{n} \right) = -qn \frac{\partial}{\partial x_i} \gamma_n, \quad (15)$$

where the term

$$\gamma_n = \frac{\hbar^2}{6mq} \frac{1}{\sqrt{n}} \frac{\partial^2}{\partial x_j^2} \sqrt{n} \quad (16)$$

is the quantum potential. Then, the conservation of momentum is given by

$$\frac{\partial}{\partial t}(mnv_i) + \frac{\partial}{\partial x_j}(mnv_i v_j + knT_n) - qn \frac{\partial}{\partial x_i} \gamma_n = -n \frac{\partial V}{\partial x_i} - \frac{mnv_i}{\tau_p}. \quad (17)$$

We can define the current density and the electric charge as  $J_j = -qnv_j$  and  $q$  is the positive electric charge. Using a diffusion scaling in (17), we obtain

$$\tau_p \frac{\partial}{\partial t} J_i - k\mu_n \frac{\partial}{\partial x_i} (nT_n) + qn\mu_n \frac{\partial}{\partial x_i} \gamma_n = \mu_n n \frac{\partial V}{\partial x_i} - J_i, \quad (18)$$

where  $\mu_n = +\frac{q\tau_p}{m}$  is the electron mobility. The potential energy is given by

$$V = -q\phi. \quad (19)$$

From (12), (18) and (19), we obtain the current continuity equation as follows:

$$\frac{1}{q} di v J_n = 0, \quad (20)$$

$$J_n = q\mu_n \left( \nabla \left( n \frac{kT_n}{q} \right) - n \nabla (\phi + \gamma_n) \right). \quad (21)$$

The energy balance equation is derived from (3) and (4) [7]. The collision term in (2) is rewritten as

$$C_p = -\frac{qv}{\mu_n}. \quad (22)$$

In analogy to (22), the collision term in (4) is modeled as

$$C_{pe} = -\frac{qS}{\mu_s}, \quad (23)$$

where  $\mu_s$  is the energy flow mobility. Neglecting the time derivative term in (2), we get

$$n\mathbf{F}_E = \nabla \cdot (nU) + n \frac{q\mathbf{v}}{\mu_n}. \quad (24)$$

Substituting (24) into (4), the expression of energy flux  $S$  is given as

$$S = \frac{\mu_s}{\mu_n} (wI + U) \cdot \mathbf{v} + \frac{\mu_s}{qn} ((wI + U) \cdot \nabla \cdot (nU) - \nabla \cdot (nR)). \quad (25)$$

Assuming a heated Maxwellian distribution, the fourth moment tensor  $R$  is specified by the classical form as

$$R = \frac{5}{2} k^2 T_n^2 I. \quad (26)$$

Using closure (26), an expression for the energy flux density  $S_n = nS$  is obtained as

$$S_n = \frac{\mu_s}{\mu_n} (wI + nU) \cdot \mathbf{v} + \frac{\mu_s}{q} \left( (wI + U) \cdot \nabla \cdot (nU) - \nabla \cdot \left( \frac{5}{2} nk^2 T_n^2 I \right) \right). \quad (27)$$

The second term of (27) is the diffusive contributions to the energy flux density which includes the classical form of  $R$ . In this work, we develop a QET model, neglecting quantum corrections in the diffusive contributions to the energy flux density. Substituting (6)–(8) into (27), the quantum corrections to the energy density  $W$  and stress tensor  $P_{ij}$  are included in the drift contributions to the energy flux density  $S_n$  and neglected in the diffusive contributions. As a result, we obtain a quantum corrected expression for the energy flux density as

$$S_n = -\frac{\mu_s}{\mu_n} \left( \frac{5}{2} \frac{kT_n}{q} - \frac{\hbar^2}{24mq} \Delta \log n - \frac{\hbar^2}{12mq} \frac{\partial^2}{\partial x_i \partial x_j} \log n \right) J_n - \frac{\mu_s}{\mu_n} \frac{5}{2} \left( \frac{k}{q} \right)^2 q\mu_n n T_n \nabla T_n. \quad (28)$$

From (3), we get

$$\nabla \cdot S_n = -J_n \cdot \nabla \phi - \frac{3}{2} kn \frac{T_n - T_L}{\tau_e}. \quad (29)$$

Assuming that the velocity  $v$  is slowly varying in the device region, the following term in (29) is approximated as

$$\frac{\hbar^2}{12m} \frac{\partial}{\partial x_i} \left( n v_j \frac{\partial^2}{\partial x_i \partial x_j} \log n \right) = \frac{\hbar^2}{12m} v_j \frac{\partial}{\partial x_i} \left( n \frac{\partial^2}{\partial x_i \partial x_j} \log n \right) + \frac{\hbar^2}{12m} \frac{\partial v_j}{\partial x_i} \left( n \frac{\partial^2}{\partial x_i \partial x_j} \log n \right) \approx -J_n \frac{\partial}{\partial x_j} \gamma_n. \quad (30)$$

Then, we obtain a four-moments QET model as follows:

$$\epsilon \Delta \varphi = q(n - p - C), \quad (31)$$

$$\frac{1}{q} \operatorname{div} J_n = 0, \quad (32)$$

$$J_n = q\mu_n \left( \nabla \left( n \frac{kT_n}{q} \right) - n \nabla (\varphi + \gamma_n) \right), \quad (33)$$

$$b_n \nabla \cdot (\rho_n \nabla u_n) - \frac{kT_n}{q} \rho_n u_n = -\frac{\rho_n}{2} (\varphi - \varphi_n), \quad (34)$$

$$\nabla \cdot S_n = -J_n \cdot \nabla \varphi - \frac{3}{2} k n \frac{T_n - T_L}{\tau_\epsilon}, \quad (35)$$

$$S_n = -\frac{\mu_s}{\mu_n} \left( \frac{5}{2} \frac{kT_n}{q} - \frac{\hbar^2}{24mq} \Delta \log n - \gamma_n \right) J_n - \frac{\mu_s}{\mu_n} \frac{5}{2} \left( \frac{k}{q} \right)^2 q \mu_n n T_n \nabla T_n, \quad (36)$$

where  $v_n = \frac{(\varphi + \gamma_n - \varphi_n)}{2}$  and  $u_n = \frac{q}{kT_n} v_n$ .  $\varphi$ ,  $\varphi_n$ , and  $p$  are the electrostatic potential, chemical potential, and hole density, respectively.  $\rho_n$  is the the root-density of electrons.  $\epsilon$ ,  $q$ , and  $k$  are the permittivity of semiconductor, electronic charge, and Boltzmann's constant.  $C$  and  $T_L$  are the ionized impurity density and the lattice temperature, respectively. The value of effective mass is given by a single parameter  $m = 0.26m_0$  in the silicon devices, where  $m_0$  is the mass of a stationary electron. The quantum parameter for electrons becomes

$$b_n = \frac{\hbar^2}{12qm}. \quad (37)$$

For a temperature dependent mobility model, we apply the simplified Hänsch's mobility model [5],

$$\frac{\mu(T_n)}{\mu_0} = \left( 1 + \frac{3}{2} \frac{\mu_0 k}{q \tau_\epsilon v_s^2} (T_n - T_L) \right)^{-1}, \quad (38)$$

where  $\mu_0$  and  $v_s$  are the low-field mobility and saturation velocity, respectively.

From (16), the quantum potential equation is derived as

$$2b_n \nabla^2 \rho_n - \gamma_n \rho_n = 0. \quad (39)$$

In our model, (39) is replaced by (34) with respect to the variable  $u_n$  by employing an exponential transformation of variable  $\rho_n = \sqrt{n} = \sqrt{n_i} \exp\left(\frac{q}{kT_n} v_n\right)$  [13]. If the variable  $u_n$  is uniformly bounded, the electron density is maintained to be positive. As mentioned below, this approach provides a numerical advantage for developing the iterative solution method of the QET model as well as the QDD model [13].

The system (31)–(36) are solved in the bounded domain  $\Omega$ . The boundary  $\partial\Omega$  of the domain  $\Omega$  splits into two disjoint part  $\Gamma_D$  and  $\Gamma_N$ . The contacts of semiconductor devices are modeled by the boundary conditions on  $\Gamma_D$ , which fulfill charge neutrality and thermal equilibrium. We further assume that no quantum effects occur at the contacts. Here, the boundary conditions are given as follows:

$$\varphi = \varphi_b + \varphi_{\text{appl}}, \quad n = n_D, \quad u_n = u_D, \quad T_n = T_L \quad \text{on } \Gamma_D, \quad (40)$$

$$\nabla \varphi \cdot \nu = \nabla J_n \cdot \nu = \nabla u_n \cdot \nu = \nabla S_n \cdot \nu = 0 \quad \text{on } \Gamma_N, \quad (41)$$

where  $\varphi_b$  is a built-in potential and  $\varphi_{\text{appl}}$  is an applied bias voltage.  $u_D = \frac{q}{kT_L} \frac{\varphi_b}{2}$  on the contacts and  $u_n = u_0$ , where  $u_0$  is a small positive constant at the silicon dioxide interface.

### 3. Discretization and iterative solution method

#### 3.1. Discretization

Space discretization of the four-moments QET model is performed by a new set of unknown variables  $(\varphi, u_n, n, T_n)$ . For the current density, we have

$$J_n = q\mu_n \left( \nabla \left( n \frac{kT_n}{q} \right) - \frac{q}{kT_n} \left( n \frac{kT_n}{q} \right) \nabla (\varphi + \gamma_n) \right). \quad (42)$$

As pointed out in discretization of classical hydrodynamic models [17,18], the total energy flow  $H = S_n + \varphi J_n$ , which consists of both the thermal energy flow  $S_n$  and the electrical flow  $\varphi J_n$ , is used to solve the energy balance equation. The total energy flow can be rewritten as

$$H = S_n + \varphi J_n = \tilde{S}_n + \left( \varphi + \frac{\mu_s}{\mu_n} \left( \frac{\hbar^2}{24mq} \Delta \log n + \gamma_n \right) \right) J_n, \tag{43}$$

$$\tilde{S}_n = -\frac{5}{2} \frac{\mu_s}{\mu_n} \frac{kT_n}{q} J_n - \frac{5}{2} \frac{\mu_s}{\mu_n} \left( \frac{k}{q} \right)^2 q \mu_n n T_n \nabla T_n. \tag{44}$$

Substituting (33) into (44), for the energy flow, we have

$$\begin{aligned} \tilde{S}_n &= -\frac{5}{2} \frac{\mu_s}{\mu_n} q \mu_n \left( \frac{kT_n}{q} \nabla n \frac{kT_n}{q} - \frac{kT_n}{q} n \nabla (\varphi + \gamma_n) + \frac{kT_n}{q} n \nabla \frac{kT_n}{q} \right) \\ &= -\frac{5}{2} q \mu_s \left( \nabla n \left( \frac{kT_n}{q} \right)^2 - \frac{q}{kT_n} n \left( \frac{kT_n}{q} \right)^2 \nabla (\varphi + \gamma_n) \right). \end{aligned} \tag{45}$$

When the variable  $\xi$  is defined as  $\xi = n \frac{kT_n}{q} = n\eta$  in the current density  $J_n$  and  $\zeta = n \left( \frac{kT_n}{q} \right)^2 = n\eta^2$  in the energy flow  $\tilde{S}_n, J_n$  and  $\tilde{S}_n$  can be written in the same form, similar as in the classical ET models [10,14],

$$\nabla \cdot F = \nabla \cdot \left( C \left( \nabla \xi - \frac{q}{kT_n} \xi \nabla (\varphi + \gamma_n) \right) \right), \tag{46}$$

where  $F$  is the flux. The constant  $C$  is defined as  $C = q\mu_n$  in  $J_n$  and  $C = -\frac{5}{2} q\mu_s$  in  $\tilde{S}_n$ . By projecting (46) onto a grid line and using the variable  $g = \int_{x_i}^x \frac{q}{kT_n} \nabla (\varphi + \gamma_n)$ , a one-dimensional self-adjoint form is obtained as

$$\frac{d}{dx} F = \frac{d}{dx} (C e^g \frac{d}{dx} (e^{-g} \zeta)). \tag{47}$$

For space discretization, the simulation region is divided into computational cells  $\Omega_{ij}$  centered at  $(x_i, y_j)$ . In a staggered Cartesian grid, each computational cell is rectangular, and the variables  $\varphi, u_n, n, T_n$  are defined at cell centers and the flux is defined at cell interfaces. For space discretization of (47), we construct high-accuracy nonlinear schemes, applying the finite-volume method to construct multidimensional schemes. For the flux  $F = C e^g \nabla (e^{-g} \zeta)$ , we integrate (47) over the computational cells  $\Omega_{ij}$ . Using Green's theorem, we obtain a discrete form as

$$\int_{\Omega_{ij}} \nabla \cdot F dx = a_j (F_{i+\frac{1}{2}} - F_{i-\frac{1}{2}}) + a_i (F_{j+\frac{1}{2}} - F_{j-\frac{1}{2}}), \tag{48}$$

where  $a_i$  and  $a_j$  are the cell sizes of the computational cell  $\Omega_{ij}$ . In order to find  $F_{i+\frac{1}{2}}$  at cell interfaces, integrating the flux  $F$  over the interval  $[x_i, x_{i+1}]$ , an approximation  $F_{i+\frac{1}{2}}$  yields

$$F_{i+\frac{1}{2}} = \frac{C (\psi_{i+1j} - \psi_{ij})}{\int_{x_i}^{x_{i+1}} e^{-g} dx}, \tag{49}$$

where  $\psi = e^{-g} \zeta$ . A similar expression is obtained for  $F_{i-\frac{1}{2}}, F_{j+\frac{1}{2}}$ , and  $F_{j-\frac{1}{2}}$ . The accuracy of the numerical flux depends on the explicit integration  $\int_{x_i}^{x_{i+1}} e^{-g} dx$  in (49). In order to construct a higher accuracy nonlinear scheme, an explicit integration  $\int_{x_i}^{x_{i+1}} e^{-g} dx$  is obtained by the piecewise linear approximation of  $\varphi$  and  $T_n$  on the interval  $[x_i, x_{i+1}]$  [15,16]. Then we have

$$F_{i+\frac{1}{2}} = \frac{C}{\theta_{i+1}^x h_{i+1}^x} \left( B(\Delta_{i+1}^x) \frac{\xi_{i+1j}^x}{\eta_{i+1j}} - B(-\Delta_{i+1}^x) \frac{\xi_{ij}^x}{\eta_{ij}} \right), \tag{50}$$

where  $B(\cdot)$  is the Bernoulli function.  $h_{i+1}^x$  is defined as  $h_{i+1}^x = (a_{i+1}^x + a_i^x)/2$ . The variables  $\theta_{i+1}^x, \Delta_{i+1}^x$  are calculated as follows:

$$\theta_{i+1}^x = \log \left( \frac{\eta_{i+1j}}{\eta_{ij}} \right) / (\eta_{i+1j} - \eta_{ij}), \tag{51}$$

$$\Delta_{i+1}^x = \theta_{i+1}^x ((\varphi_{i+1j} - \varphi_{ij}) + (\gamma_{n_{i+1j}} - \gamma_{n_{ij}}) - (\eta_{i+1j} - \eta_{ij})). \tag{52}$$

Such schemes to  $J_n$  and  $\tilde{S}_n$  result in a consistent generalization of the Scharfetter–Gummel type schemes to the QET equations. The energy balance equation is further discretized using (49). To conserve the total energy flow  $H = S_n + \varphi J_n$  (43), discretization of the carrier heating term is another key issue [17,18]. Integrating (35) over the computational cell yields

$$\begin{aligned} &\int_{\Omega_{ij}} \nabla \cdot \tilde{S}_n dx \\ &= \int_{\Omega_{ij}} -J_n \cdot \nabla \left( \varphi + \frac{\mu_s}{\mu_n} \left( \gamma_n + \frac{b_n}{2} \Delta \log n \right) \right) dx - \int_{\Omega_{ij}} \frac{3}{2} kn \frac{T_n - T_L}{\tau_\epsilon} dx. \end{aligned} \tag{53}$$

Here, quantum corrections are included in the carrier heating term. From Gauss's theorem, the first term on the right hand side of (53) can be calculated as

$$\int_{\Omega_{ij}} -J_n \cdot \nabla \left( \varphi + \frac{\mu_s}{\mu_n} \left( \gamma_n + \frac{b_n}{2} \Delta \log n \right) \right) dx = - \int_{\partial\Omega_{ij}} \left( J_n \left( \varphi + \frac{\mu_s}{\mu_n} \left( \gamma_n + \frac{b_n}{2} \Delta \log n \right) \right) \right) \cdot v dx. \tag{54}$$

Assuming the Boltzmann statics, the electron density is expressed as

$$n = n_i \exp \left( \frac{q(\varphi + \gamma - \varphi_n)}{kT_n} \right) = n_i \exp(2u_n), \tag{55}$$

where  $n_i$  is the intrinsic density. Then, the discretization for  $\Delta \log n = 2\Delta u_n$  in (54) is obtained by a standard five-point approximation:

$$\Delta^h u_n^h = \frac{1}{a_j^y h_{j+1}^y} u_{i,j+1} + \frac{1}{a_j^y h_j^y} u_{i,j-1} + \frac{1}{a_i^x h_{i+1}^x} u_{i+1,j} + \frac{1}{a_i^x h_i^x} u_{i-1,j} - \left( \frac{h_{j+1}^y + h_j^y}{a_j^y h_{j+1}^y h_j^y} + \frac{h_{i+1}^x + h_i^x}{a_i^x h_{i+1}^x h_i^x} \right) u_{i,j}. \tag{56}$$

The discrete form of the carrier heating term in (53) yields

$$\begin{aligned} \int_{\Omega_{ij}} -J_n \cdot \nabla \left( \varphi + \frac{\mu_s}{\mu_n} (\gamma_n + b_n \Delta^h u_n^h) \right) dx \approx & -a_i^x \left( J_{n_{j+\frac{1}{2}}} \left( \varphi_{j+\frac{1}{2}} + \frac{\mu_s}{\mu_n} (\gamma_{n_{j+\frac{1}{2}}} + b_n \Delta^h u_n^h) \right) \right. \\ & \left. - J_{n_{j-\frac{1}{2}}} \left( \varphi_{j-\frac{1}{2}} + \frac{\mu_s}{\mu_n} (\gamma_{n_{j-\frac{1}{2}}} + b_n \Delta^h u_n^h) \right) \right) - a_j^y \left( J_{n_{i+\frac{1}{2}}} \left( \varphi_{i+\frac{1}{2}} + \frac{\mu_s}{\mu_n} (\gamma_{n_{i+\frac{1}{2}}} + b_n \Delta^h u_n^h) \right) \right. \\ & \left. - J_{n_{i-\frac{1}{2}}} \left( \varphi_{i-\frac{1}{2}} + \frac{\mu_s}{\mu_n} (\gamma_{n_{i-\frac{1}{2}}} + b_n \Delta^h u_n^h) \right) \right). \end{aligned} \tag{57}$$

Space discretization of (34) is performed following our previous works [13,19] to achieve a Scharfetter–Gummel type scheme, i.e.,

$$\begin{aligned} & \frac{a_j^y}{h_{i+1}^x} b_n e^{u_{n_{i+1,j}}} B(u_{n_{i+1,j}} - u_{n_{i,j}})(u_{n_{i+1,j}} - u_{n_{i,j}}) - \frac{a_j^y}{h_i^x} b_n e^{u_{n_{i,j}}} B(u_{n_{i,j}} - u_{n_{i-1,j}})(u_{n_{i,j}} - u_{n_{i-1,j}}) + \frac{a_i^x}{h_{j+1}^y} b_n e^{u_{n_{i,j+1}}} B(u_{n_{i,j+1}} - u_{n_{i,j}})(u_{n_{i,j+1}} \\ & - u_{n_{i,j}}) - \frac{a_i^x}{h_j^y} b_n e^{u_{n_{i,j}}} B(u_{n_{i,j}} - u_{n_{i,j-1}})(u_{n_{i,j}} - u_{n_{i,j-1}}) - \eta_{ij} u_{n_{ij}} \Lambda_{ij} \\ & = -\frac{1}{2} (\varphi_{ij} - \varphi_{n_{ij}}) \Lambda_{ij}, \end{aligned} \tag{58}$$

where  $\Lambda_{ij} = \int_{\Omega_{ij}} \rho_n dx$ , which is approximated as

$$\Lambda_{ij} = \frac{1}{4} e^{u_{n_{ij}}} \times \left( \frac{h_i^x h_j^y}{B(\frac{u_{i-1,j}-u_{ij}}{2}) B(\frac{u_{ij}-u_{i+1,j}}{2})} + \frac{h_{i+1}^x h_j^y}{B(\frac{u_{i+1,j}-u_{ij}}{2}) B(\frac{u_{ij}-u_{i-1,j}}{2})} + \frac{h_i^x h_{j+1}^y}{B(\frac{u_{i,j}-u_{ij}}{2}) B(\frac{u_{ij}-u_{i,j+1}}{2})} + \frac{h_{i+1}^x h_j^y}{B(\frac{u_{i+1,j}-u_{ij}}{2}) B(\frac{u_{ij}-u_{i,j-1}}{2})} \right). \tag{59}$$

### 3.2. Iterative solution method

We develop an iterative solution method of the QET model by constructing a Gummel map [20] with a new set of unknown variables  $(\varphi, u_n, n, T_n)$  as follows:

**(P1)** Let  $\varphi^m, n^m, p^m, T_n^m$  are given, solve the nonlinear Poisson equation with respect to the electrostatic potential  $\varphi^{m+1}$ , where  $m$  is the number of iteration. Eq. (31) is linearized using a Newton method. Then the linearized equation becomes

$$\epsilon \Delta \varphi^{m+1} - \frac{q^2}{k} \left( \frac{n^m}{T_n^m} + \frac{p}{T_p} \right) \varphi^{m+1} = q(n^m - p^m - C) - \frac{q^2}{k} \left( \frac{n^m}{T_n^m} + \frac{p}{T_p} \right) \varphi^m. \tag{60}$$

**(P2)** Let  $\varphi^{m+1}, S^m, \varphi_n^m, T_n^m$  are given, solve the potential  $u_n^{m+1}$ .

$$b_n \nabla \cdot (\rho_n^m \nabla u_n^{m+1}) - \eta^m \rho_n^m u_n^{m+1} = -\frac{\rho_n^m}{2} (\varphi^{m+1} - \varphi_n^m). \tag{61}$$

Then, using  $u_n^{m+1}$  the quantum potential is further calculated as

$$\gamma_n^{m+1} = 2\eta^m u_n^{m+1} + \varphi_n^m - \varphi^{m+1}. \tag{62}$$

**(P3)** Let  $\varphi^{m+1}, \gamma_n^{m+1}, T_n^m$  are given, solve the electron density  $n^{m+1}$ .

$$\frac{1}{q} \operatorname{div} J_n = 0, \tag{63}$$

$$J_n = q \mu_n e^g \nabla (e^{-g} n^{m+1} \eta^m). \tag{64}$$

We set the generalized chemical potential by

$$\varphi_n^m = -\eta^m \log \frac{n^{m+1}}{n_i} + \varphi^{m+1} + \gamma_n^{m+1}. \tag{65}$$

(P4) Let  $\varphi^{m+1}, \gamma_n^{m+1}, n^{m+1}, T_n^m$  are given, solve the electron temperature  $T_n^{m+1}$ .

$$\begin{aligned} \nabla \cdot \tilde{S}_n + \frac{3}{2} k \frac{n^{m+1} T_n^{m+1}}{\tau_\epsilon} \\ = -J_n \cdot \nabla \left( \varphi^{m+1} + \frac{\mu_s}{\mu_n} (\gamma_n^{m+1} + b_n \Delta u_n^{m+1}) \right) + \frac{3}{2} k \frac{n^{m+1} T_L}{\tau_\epsilon}. \end{aligned} \tag{66}$$

An iterative solution method, which consists of the inner and outer iteration loops, is developed, as shown in Fig. 1. The algorithm using the variable  $u_n$  in (34) ensures the positivity of the root-density of electrons without introducing damping parameters [13]. In fact, it is a critical issue to solve for the root-density  $\rho_n$  the quantum potential equation

$$-2b_n \nabla^2 \rho_n + \gamma_n \rho_n = 0. \tag{67}$$

In this case, the iterative solution method requires an additional iteration loop to maintain positive solutions for the root-density of electrons in the inner iteration loop as pointed out in Ref. [21]. Hence, in the inner iteration loop, (67) is replaced by (34). Therefore, we can enhance the robustness of the iterative solution method by introducing an under relaxation method with a parameter  $\alpha$ ,  $0 < \alpha < 1$ , in the outer iteration loop:

$$T^{m+1} = T^m + \alpha(T_*^{m+1} - T^m). \tag{68}$$

The convergence behavior of electron temperature is shown in Fig.2 as a function of the relaxation parameter. It is clear that the numerical stability is obtained by the relaxation method.

### 4. Numerical results

The numerical results are obtained for a 35 nm MOSFET having thin gate oxide thickness of 1.5 nm, uniform substrate concentration of  $2.0 \times 10^{18} \text{ cm}^{-3}$ , and n-type doping concentration of  $1.0 \times 10^{20} \text{ cm}^{-3}$ . The energy relaxation time  $\tau_\epsilon$  of  $0.1 \times 10^{-12}$  ps and a ratio  $\mu_s/\mu_n$  of 0.8 are chosen. The MOSFET structure is shown in Fig. 3. The QET model includes a

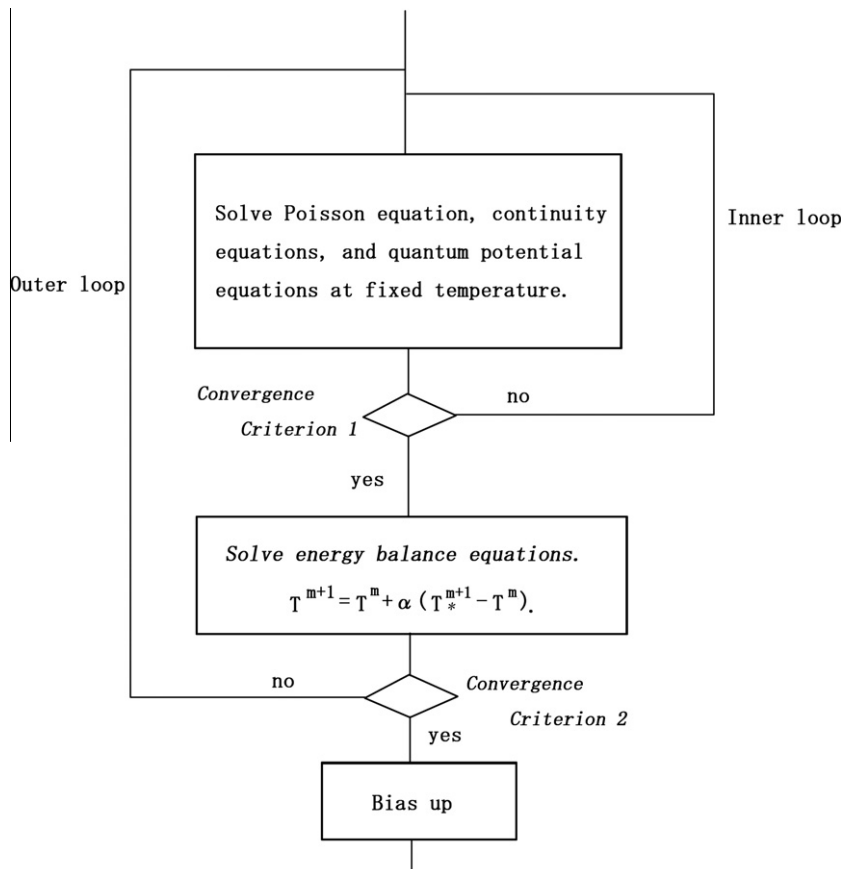


Fig. 1. An iterative solution method with a relaxation algorithm.

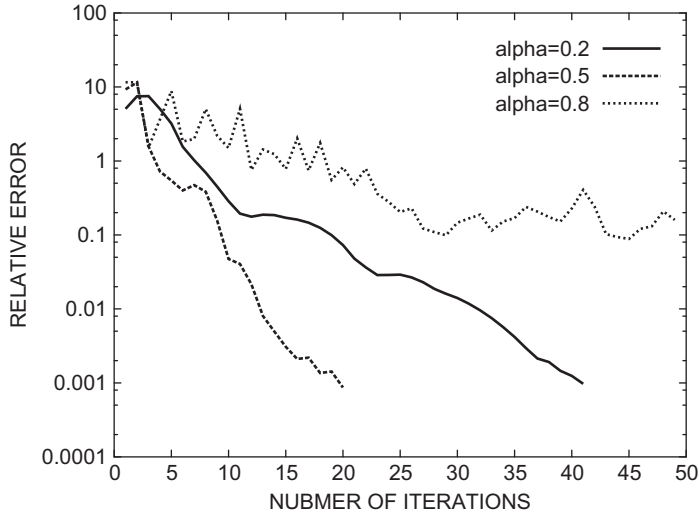


Fig. 2. Relative error of electron temperature vs. number of iterations at different relaxation parameters.

two-dimensional calculation of the electrostatic potential in the region with boundary A-G-L-F, and a two-dimensional calculation of the variables  $n$ ,  $u_n$ , and  $T_n$  in the silicon region with boundary A-B-E-F. The mixed boundary conditions for the QET system are assigned as follows:

For the electrostatic potential  $\varphi$

$$\varphi = \varphi_{appl} + \varphi_b, \tag{69}$$

at source and drain regions, and back gate, where  $\varphi_{appl}$  is the applied bias voltage, and  $\varphi_b$  is the built-in potential, respectively. The gate region is also treated as a Dirichlet boundary condition with an approximated work function of the material. At the sides A-B, H-I, J-K, E-F, we have the homogeneous Neumann condition

$$\frac{\partial \varphi}{\partial \nu} = 0. \tag{70}$$

For the variables  $n$ ,  $u_n$ , and  $T_n$ , we have the constant Dirichlet conditions

$$n = \begin{cases} (C + \sqrt{C^2 + 4n_i^2})/2 & \text{at sides } B-C \text{ and } D-E, \\ 2n_i^2/(-C + \sqrt{C^2 + 4n_i^2}) & \text{at the back gate,} \end{cases}$$

$$T_n = T_L \text{ at sides } B-C, D-E, \text{ and } A-F,$$

$$u_n = \begin{cases} (q\varphi_b)/(2kT_n) & \text{at sides } B-C, D-E, \text{ and } A-F, \\ u_0 & \text{at the silicon-oxide interface } C-D, \end{cases} \tag{71}$$

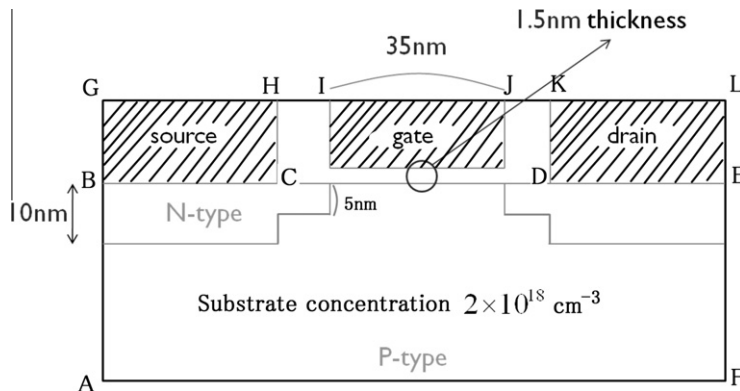


Fig. 3. Two-dimensional cross section of a 35 nm MOSFET.

where  $u_0$  is the small positive constant. At the sides A–B and E–F, the homogeneous Neumann conditions read:

$$\frac{\partial n}{\partial v} = \frac{\partial T_n}{\partial v} = \frac{\partial u_n}{\partial v} = 0, \tag{72}$$

at the side C–D,

$$\frac{\partial n}{\partial v} = \frac{\partial T_n}{\partial v} = 0. \tag{73}$$

In Fig. 4 and Fig. 5, we compare the electron density distributions calculated by QDD, QET and classical ET models. The device was biased with  $V_g = 0.8$  V and  $V_d = 0.8$  V. The simulated density distributions are plotted at different positions of the channel. Fig. 4 shows the electron density distributions perpendicular to the interface at the source end of the channel. The electron density distributions calculated from the QET and QDD models are almost identical in the inversion layers. Carrier heating due to the short channel effects results in the spread of electrons towards the bulk in simulations using the QET and ET models. As a result, the profiles between two models are almost identical at the bulk. The electron density distributions

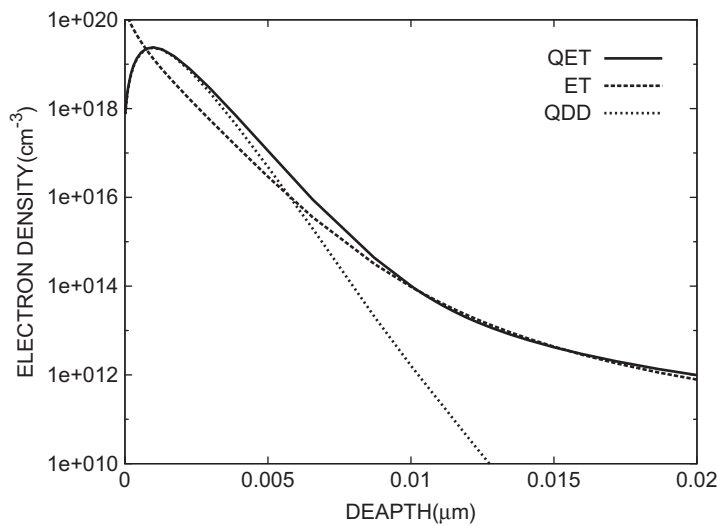


Fig. 4. Electron density distributions perpendicular to the interface at the source end of the channel for a 35 nm MOSFET.

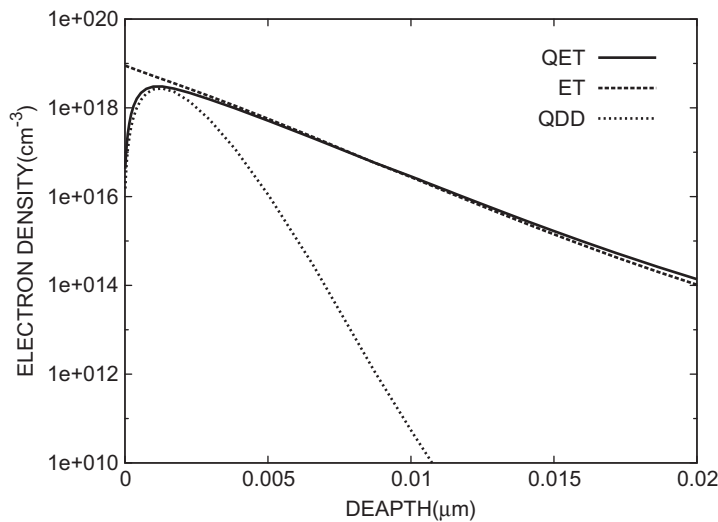
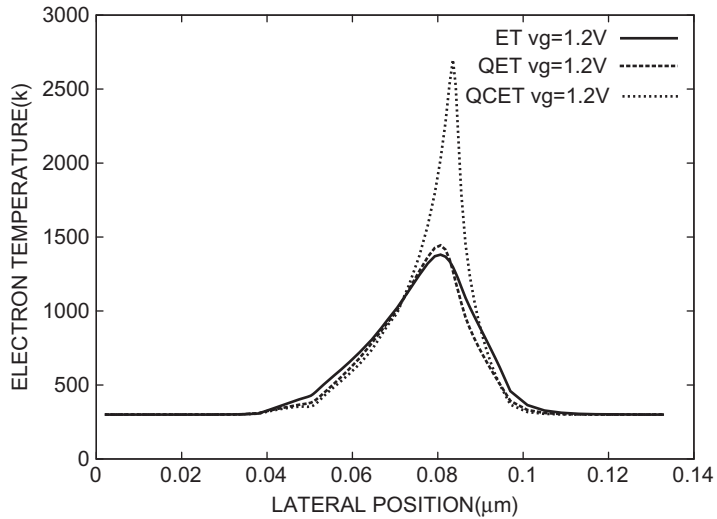
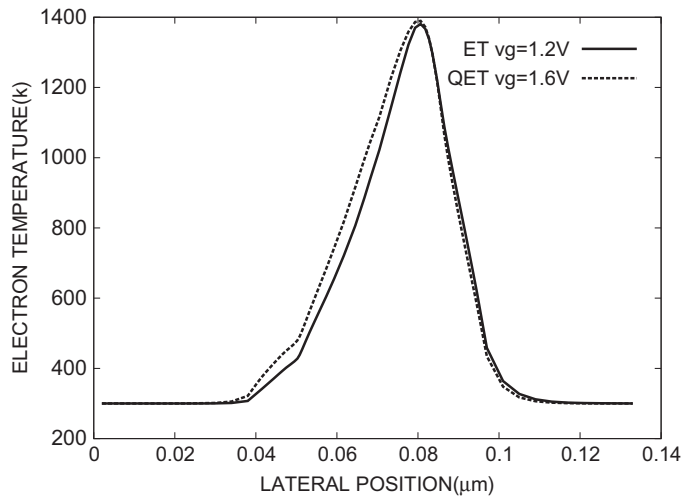


Fig. 5. Electron density distributions perpendicular to the interface at the drain end of the channel for a 35 nm MOSFET.



**Fig. 6.** Lateral profiles of electron temperature distributions calculated by ET (solid line), QET, and QCET models at the same drain bias of  $V_d = 0.8$  V and the same gate bias of  $V_g = 1.2$  V.



**Fig. 7.** Lateral profiles of electron temperature distributions calculated by ET (solid line) and QET (dotted line) models at the same drain bias of  $V_d = 0.8$  V. ET model at  $V_g = 1.2$  V, QET model at  $V_g = 1.6$  V.

perpendicular to the interface at the drain end of the channel are shown in Fig. 5. The results clearly indicate that the quantum confinement effect is reduced by the enhanced diffusion towards the bulk due to the high electron temperature near the drain. The QET model allows simulations of quantum confinement transport with hot-carrier effects in MOSFETs.

Fig. 6 shows lateral profiles of electron temperature calculated by the QET, QCET, and ET models at the same gate voltage of 1.2 V. In Fig. 7, we compare the results calculated by the ET model at  $V_g = 1.2$  V and the QET model at  $V_g = 1.6$  V. The simulations are done at the same drain voltage of 0.8 V. The quantum corrected ET (QCET) model is a simplified QET model based on [4] with a temperature dependent mobility model (38). In the QCET model, the quantum correction to the energy density is neglected, and the carrier temperature in the current density is approximated by the lattice temperature [4]. As shown in Fig. 6, the QET model exhibits a sharper distribution of electron temperature at the lateral direction, when compared to that calculated by the classical ET model. The electron temperature calculated by the QCET model is further increased. This difference is caused by the threshold voltage shift due to the quantum confinement transport in the channel. Therefore, as shown in Fig. 7, the shape of electron temperature distributions calculated by the QET model at  $V_g = 1.6$  V is close to that obtained by the ET model at  $V_g = 1.2$  V. In Fig. 8, we present the  $x$ -component of the current densities calculated by the QET and ET models. The results verify that the magnitude of the current density calculated by the QET model at  $V_g = 1.6$  V corresponds to that calculated by the ET model at  $V_g = 1.2$  V.

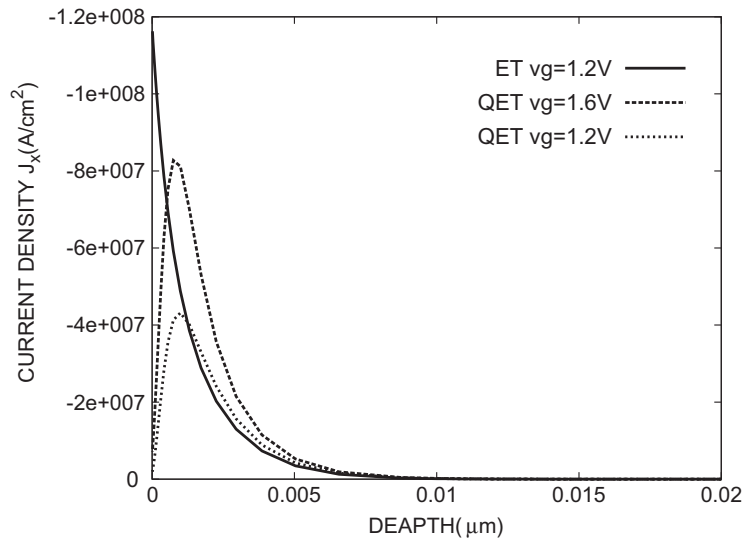


Fig. 8. x-Component of current densities perpendicular to the interface for a 35 nm MOSFET. ET model at  $V_g = 1.2$  V, QET model at  $V_g = 1.2$  V and  $V_g = 1.6$  V.

## 5. Conclusion

A four-moments QET model has been derived by using a diffusion scaling in the quantum hydrodynamic model. Space discretization of the four-moments QET model has been performed by a new set of unknown variables. Numerical schemes result in a consistent generalization of the Scharfetter-Gummel type scheme to the QET equations. We can enhance the robustness of the iterative solution method by introducing a relaxation method. The QET model allows simulations of quantum confinement transport with hot-carrier effects in scaled MOSFETs. The simulation results reveal the difference of electron temperature distributions between the QET and ET models due to the quantum confinement effects.

## Acknowledgement

The authors thank Dr. Shimada for numerical simulations.

## References

- [1] P. Degond, F. Méhats, C. Ringhofer, Quantum energy transport and drift diffusion models, *J. Stat. Phys.* 118 (2005) 625–667.
- [2] G. Allaire, A. Arnold, P. Degond, T.Y. Hou, *Quantum Transport*, Springer, 2008, pp. 144–152.
- [3] S. Jin, Y.-J. Park, H.-S. Min, Simulation of quantum effects in the nano-scale semiconductor device, *J. Semi. Tech. Sci.* 4 (2004) 32–38.
- [4] R.-C. Chen, J.-L. Liu, An accelerated monotone iterative method for the quantum-corrected energy transport model, *J. Comp. Phys.* 204 (2005) 131–156.
- [5] T. Grasser, T.-W. Tang, H. Kosina, S. Selberherr, A review of hydrodynamic and energy-transport models for semiconductor device simulation, *IEEE Proc.* 91 (2003) 251–274.
- [6] C.L. Gardner, The quantum hydrodynamic model for semiconductor devices, *SIAM J. Appl. Math.* 24 (1994) 409–427.
- [7] S.-C. Lee, T.-W. Tang, Transport coefficients for a silicon hydrodynamic model extracted from inhomogeneous monte-carlo calculations, *Solid-State Elec.* 35 (1992) 561–569.
- [8] A. Bringer, G. Schön, Extended moment equations for electron transport in semiconducting submicron structures, *J. Appl. Phys.* 64 (1988) 2447–2455.
- [9] R. Thoma, A. Emunds, B. Meinerzhagen, H.J. Peifer, W.L. Engl, Hydrodynamic equations for semiconductors with nonparabolic band structure, *IEEE Trans. Electron Devices* 38 (1991) 1343–1353.
- [10] M. Gritsch, H. Kosina, T. Grasser, S. Selberherr, Revision of the standard hydrodynamic transport model for SOI simulation, *IEEE Trans. Electron Devices* 49 (2002) 1814–1820.
- [11] M.G. Ancona, G.J. Iafrate, Quantum correction to the equation of state of an electron gas in a semiconductor, *Phys. Rev. B* 39 (1989) 9536–9540.
- [12] E. Wigner, On the quantum correction for thermodynamic equilibrium, *Phys. Rev.* 40 (1932) 749–759.
- [13] S. Odanaka, Multidimensional discretization of the stationary quantum drift-diffusion model for ultrasmall MOSFET structures, *IEEE Trans. CAD ICAS* 23 (2004) 837–842.
- [14] B. Meinerzhagen, W.-L. Engl, The influence of the thermal equilibrium approximation on the accuracy of classical two-dimensional numerical modeling of silicon submicrometer MOS transistors, *IEEE Trans. Electron Devices* 35 (1988) 689–697.
- [15] M. Rudan, F. Odeh, Multi-dimensional discretization scheme for the hydrodynamic model of semiconductor devices, *COMPEL* 5 (3) (1986) 149–183.
- [16] T.-W. Tang, Extension of the Scharfetter-Gummel algorithm to the energy balance equation, *IEEE Trans. Electron Devices* ED-31 (1984) 1912–1914.
- [17] A. Forghieri, R. Guerrieri, P. Ciampolini, A. Gnudi, M. Rudan, G. Baccarani, A new discretization strategy of the semiconductor equations comprising momentum and energy balance, *IEEE Trans. Comput. Aided Des.* 7 (1988) 231–242.
- [18] D. Chen, E.-C. Kan, U. Ravaioli, C.-W. Shu, R.-W. Dutton, An improved energy transport model including nonparabolicity and non-Maxwellian distribution effects, *IEEE Electron Device Lett.* 13 (1992) 26–28.
- [19] S. Odanaka, A high-resolution method for quantum confinement transport simulations in MOSFETs, *IEEE Trans. CAD ICAS* 26 (2007) 80–85.
- [20] H.K. Gummel, A self-consistent iterative scheme for one-dimensional steady state transistor calculations, *IEEE Trans. Electron Devices* 11 (1964) 455–465.
- [21] C. de Falco, E. Gatti, A.L. Lacaita, R. Sacco, Quantum-corrected drift-diffusion models for transport in semiconductor devices, *J. Comput. Phys.* 204 (2005) 533–561.